

# Fabrication of Multilayer Systems Combining Microfluidic and Microoptical Elements for Fluorescence Detection

Jean-Christophe Roulet, Reinhard Völkel, Hans Peter Herzig, Elisabeth Verpoorte, Nico F. de Rooij, *Senior Member, IEEE*, and René Dändliker

**Abstract**—This paper presents the fabrication of a microchemical chip for the detection of fluorescence species in microfluidics. The microfluidic network is wet-etched in a Borofloat 33 (Pyrex) glass wafer and sealed by means of a second wafer. Unlike other similar chemical systems, the detection system is realized with the help of microfabrication techniques and directly deposited on both sides of the microchemical chip. The detection system is composed of the combination of refractive microlens arrays and chromium aperture arrays. The microfluidic channels are 60  $\mu\text{m}$  wide and 25  $\mu\text{m}$  deep. The utilization of elliptical microlens arrays to reduce aberration effects and the integration of an intermediate (between the two bonded wafers) aluminum aperture array are also presented. The elliptical microlenses have a major axis of 400  $\mu\text{m}$  and a minor axis of 350  $\mu\text{m}$ . The circular microlens diameters range from 280 to 300  $\mu\text{m}$ . The apertures deposited on the outer chip surfaces are etched in a 3000-Å-thick chromium layer, whereas the intermediate aperture layer is etched in a 1000-Å-thick aluminum layer. The overall thickness of this microchemical system is less than 1.6 mm. The wet-etching process and new bonding procedures are discussed. Moreover, we present the successful detection of a 10-nM Cy5 solution with a signal-to-noise ratio (SNR) of 21 dB by means of this system. [644]

**Index Terms**—Fluorescence detection, glass-to-glass bonding,  $\mu\text{TAS}$ , refractive microlens, wet etching.

## I. INTRODUCTION

TO DATE, various types of miniaturized systems for chemical analysis in microfluidic channels have been realized with the help of microfabrication techniques. The detection modes in these systems can be as varied as ultraviolet (UV)-absorbance [1]–[3], refractive index measurements [4], [5], electrochemical detection [6]–[8], or laser-induced fluorescence detection (LIF) [9], [10]. Due to its selectivity and high sensitivity [11]–[13], LIF is one of the preferred detection techniques on microchemical chips. For multichannel chips, the most commonly used strategy today is to scan the analytical chip with respect to a stationary detection system (such as confocal microscopy) or to sweep the channels with a light beam [14]. These solutions require precise, and thus often expensive, bulky

mechanical and optical systems, such as translation stages, movable mirrors, or confocal microscopes. Though microfabricated forms of some of these elements exist [15], [16], they do not allow the scanning of a large number of microfluidic channels (or microchannels) evenly distributed on a 100-mm wafer. Moreover, they are difficult to integrate, and hence not suitable for the realization of micro total analysis systems ( $\mu\text{TAS}$ ).

These are the reasons why we take advantage of microfabrication technology to directly integrate the detection system onto the chemical chip. This solution enables the fabrication of small and closely spaced optical elements, their precise alignment with respect to the microfluidics, and the realization of original detection system configurations [17], [18]. A chemical chip with partially integrated optical elements was previously realized [19]. This chip was made of a 100-mm-diameter 0.5-mm-thick glass wafer in which microfluidic networks were patterned and sealed by a second identical wafer. The optical detection system was composed of an array of refractive photoresist microlenses and conventional aluminum pinholes. The microlenses for illumination were microfabricated on one side of the chemical chip, whereas the those for collection of fluorescence light were formed on a separate glass wafer. The separate wafer was sawn, then precisely aligned under a microscope and glued with the help of a UV-curable glue on the collection side of the chemical chip. In the same way, two chromium pinholes were affixed on both sides of the system. A signal emitted by a solution of 20-nM Cy5<sup>1</sup> was recorded with this system. However, it was clear that manually assembling the microoptical components limited alignment precision and hence detection performance. Microfabrication was required in order to get precise alignment and a perfect size match of all the different elements to decrease stray light and increase the signal-to-noise ratio (SNR).

The new chip presented here is made up of a 0.5-mm-thick cover wafer and a 1-mm-thick wafer in which the microfluidic network is patterned. Both wafers are 100 mm in diameter. As shown in Fig. 1, two patterned chromium layers and refractive microlenses deposited directly on both sides of the chemical chip form the detection system. The photoresist microlenses are fabricated by a resist melting technique [20], [21]. The microchip was designed for biochemical analysis using a heterogeneous immunoassay technique [22]. The microfluidic network is patterned by photolithography and etched with hydrofluoric acid

Manuscript received November 13, 2000; revised May 1, 2001. This work was supported by the Swiss Priority Program "Micro- and Nanosystems Technology" (MINAST). Subject Editor A. J. Ricco.

J.-C. Roulet, H. P. Herzig, E. Verpoorte, N. F. de Rooij, and R. Dändliker are with the Institute of Microtechnology, University of Neuchâtel, CH-2000 Neuchâtel, Switzerland (e-mail: jean-christophe.roulet@unine.ch).

R. Völkel is with Karl Süss Neuchâtel, 2007 Neuchâtel, Switzerland.

Publisher Item Identifier S 1057-7157(01)06794-4.

<sup>1</sup>Amersham Life Science Ltd., Bucks, U.K.

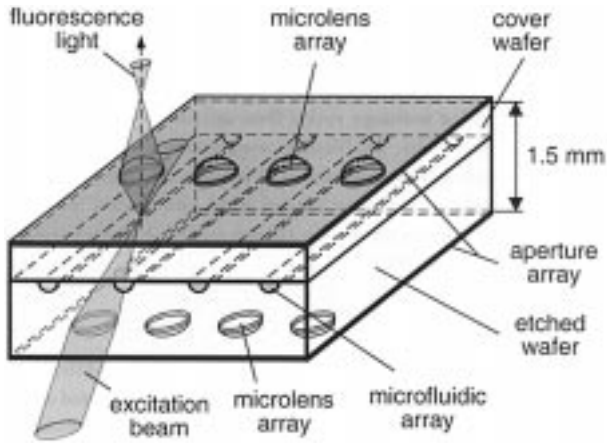


Fig. 1. Microchip configuration. An excitation beam, focused by a first microlens, and the fluorescence light collected by a second microlens are also presented for one channel. For the sake of clarity, microlens and microfluidic arrays are drawn larger than in reality.

(HF) [23], [24], as will be discussed below. Fig. 2(a) presents the detection principle. The incoming laser beam is first focused into a 60- $\mu\text{m}$ -wide 25- $\mu\text{m}$ -deep microchannel with the help of a first microlens. In the case of a laser beam diameter bigger than the entrance microlens diameter, the light passing around the microlens is not focused into the microchannel and hence is not usable for dye excitation. Moreover, it is an important source of background signal. This is why an entrance aperture layer is used to block this part of the laser beam. On the other side of the chip, a microlens collects and focuses the fluorescence light emitted from the microchannel onto the detector. The second aperture layer (exit aperture layer) prevents the unabsorbed excitation beam from being scattered onto the detector. Fig. 2(b) shows a similar system, but with a third aperture array forming an intermediate layer between the two glass wafers. The function of this intermediate aperture layer is to block the part of the excitation beam scattered at the level of the entrance microlens that is not focused into the microfluidic channel, and hence to reduce the stray light.

The SNR (power of the background-corrected signal/noise power) and SNR in dB are given by [25]

$$\text{SNR} = \frac{(\bar{S}_F - \bar{S}_B)^2}{\sigma_F^2 + \sigma_B^2} \quad (1)$$

and

$$\text{SNR}_{dB} = 10 \log \frac{(\bar{S}_F - \bar{S}_B)^2}{\sigma_F^2 + \sigma_B^2} \quad (2)$$

where  $\bar{S}_F$  and  $\bar{S}_B$  are the average fluorescence and background signal, respectively, and  $\sigma_F$  and  $\sigma_B$  are the variances of  $\bar{S}_F$  and  $\bar{S}_B$ , respectively. The total noise is hence calculated as the sum of the variances  $\sigma_F^2$  and  $\sigma_B^2$ . The off-axis illumination scheme as presented in Fig. 2(a) and (b) enables a geometrical separation between the excitation beam and the fluorescence light collected by the second microlens. In an ideal case, spectral filtering (e.g., with an interference filter) would not be necessary. Part of the excitation beam is, however, scattered at entrance microlens and microchannel interfaces. Some excitation light

is therefore collected by the second microlens (the one used to collect the fluorescence light), increasing the background signal level. Since the SNR is inversely proportional to the background signal level  $\bar{S}_B$ , a reduction of  $\bar{S}_B$  increases the SNR and hence reduces the limit of detection (LOD). The LOD is defined as the fluorochrome concentration giving a signal with an SNR of nine. An interference filter is placed in front of the photodetector in order to improve the separation between the fluorescence light and the collected part of the excitation beam. Such detection schemes combining geometrical and spectral separation enable the detection of lower concentrations than detection systems based only on interference filters [18].

The techniques used for the realization of the microchemical chips and for the optical detection system deposition presented in this paper are commonly used microfabrication techniques and hence do not require special equipment. The Pyrex wafers necessary for the realization of microchemical chips enabling the integration of optical detection systems working in the visible are, however, somewhat more expensive than silicon wafers. The systems presented in Fig. 2(a) and (b) require only five and six photolithographic steps, respectively.

## II. CHEMICAL CHIP FABRICATION

### A. Wet Etching

As discussed in Section I, to reach high detection sensitivity and low LOD, the background signal level  $\bar{S}_B$  must be as low as possible. Therefore, the amount of excitation light collected by the second microlens must be as low as possible. This is why particular attention must be paid to excitation beam scattering sources and hence to the surface roughness of the microchannels. The main chemical chip fabrication steps are summarized in Fig. 3. The etching process begins by cleaning the wafers for 10 min in 100% fuming nitric acid ( $\text{HNO}_3$ ). The wafers are then carefully rinsed with deionized (DI) water in a cascade bath and dried with pressurized nitrogen. A wet-etching mask of a 2000- $\text{\AA}$  polysilicon (poly-Si) layer is first deposited on both sides of the 1-mm-thick wafer by low-pressure chemical vapor deposition (LPCVD). A 1.5- $\mu\text{m}$ -thick AZ1518<sup>2</sup> photoresist layer is then spin-coated on one side of the wafer. After prebaking (85  $^\circ\text{C}$ , 35 min), the photoresist is exposed through a chromium mask (Fig. 4) with the help of an AL6-2 mask aligner.<sup>3</sup> After development in an AZ351B solution,<sup>4</sup> the wafer is rinsed with DI water and dried with pressurized nitrogen. The patterned photoresist layer is then hardened (120  $^\circ\text{C}$ , 30 min) and the unprotected poly-Si layer removed by reactive ion etching (RIE). The photoresist is stripped with MOS-quality acetone. The wafer is then rinsed with MOS-quality isopropanol and dried with pressurized nitrogen. To get rid of all the photoresist traces and RIE redeposition products, the procedure is completed by a 10-min oxygen plasma cleaning (100 mTorr, 100  $^\circ\text{C}$ ). The microfluidic network is then isotropically etched in 20% HF at cleanroom temperature (21  $^\circ\text{C}$ ). The etching time is  $\sim 22$  min (etching rate  $\sim 1.1 \mu\text{m}/\text{min}$ ). The etching process is followed by a thorough rinse with DI water. The poly-Si mask

<sup>2</sup>Clariant AG, Muttensz, Switzerland.

<sup>3</sup>Karl Süss KG, München, Germany.

<sup>4</sup>Clariant AG, Muttensz, Switzerland.

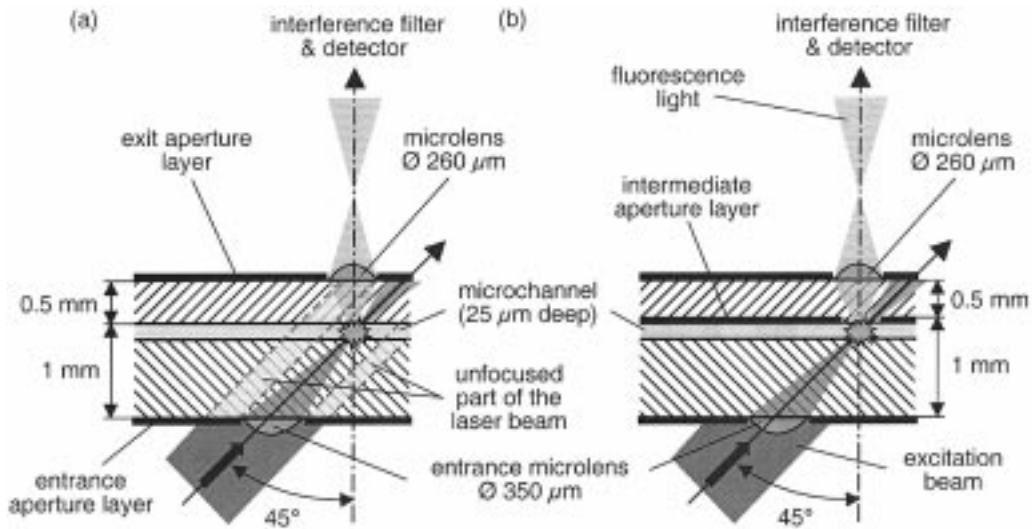


Fig. 2. Detection principle. (a) System without intermediate aperture layer. (b) System with intermediate aperture layer, which is composed of a patterned Al layer covered by a PECVD  $\text{Si}_3\text{N}_4$  layer.

is then removed in a 60 °C KOH bath (2 min), followed by a rinse in DI water.

The 0.5-mm-thick cover wafers have 1 mm ultrasonically drilled holes to enable access to microfluidic networks. If an intermediate aperture layer is needed, an LPCVD of a 1000-Å aluminum layer is performed on one side of the cover wafers. The aluminum layer is patterned by means of the same photolithographic technique as used to pattern the poly-Si layer, except that the aluminum layer is etched in an AZ400K<sup>5</sup> solution for 5 min. Any Al deposited in the access holes is removed during this step. A 1000-Å plasma-enhanced chemical-vapor-deposited (PECVD) silicon nitride ( $\text{Si}_3\text{N}_4$ ) layer then covers the aluminum layer. This nonconducting layer not only enables wafer bonding but also isolates electrically the microfluidic channels, which is necessary for electroosmotic pumping and capillary electrophoresis separation (requiring high potentials between the inlets). Moreover, the nonconducting layer must enable the transmission of the fluorescence light emitted by the fluorochrome solution in the microchannel to the detector [Fig. 2(b)] and therefore be transparent at the fluorochrome emission wavelength. ( $\text{Si}_3\text{N}_4$ ) has been chosen because of its wide transparency window ranging from 290 to 9000 nm [26] enabling the utilization of a wide range of fluorochromes. The Cy5 fluorochrome used here has an emission peak at  $\sim 670$  nm. Silicon dioxide ( $\text{SiO}_2$ ) and silicon carbide (a-SiC:H) are also good alternatives to the silicon nitride insulating layer [27], [28].

To test the fabrication of systems with intermediate aperture arrays and to avoid the cost of a chromium mask, the aperture pattern is printed on a transparent polyester film<sup>6</sup> with a resolution of 3600 dpi. This film is then taped onto an old 5-in mask from which the chromium layer has been removed. Both the microfluidic wafer and the cover wafer are made of Borofloat 33 glass,<sup>7</sup> which is equivalent to Corning 7740 (Pyrex). Wafer

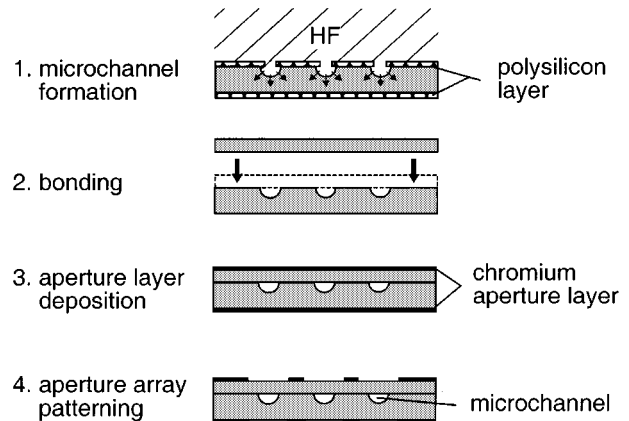


Fig. 3. Schematic diagram of microchemical chip fabrication and aperture-layer deposition (for the case without intermediate aperture layer).

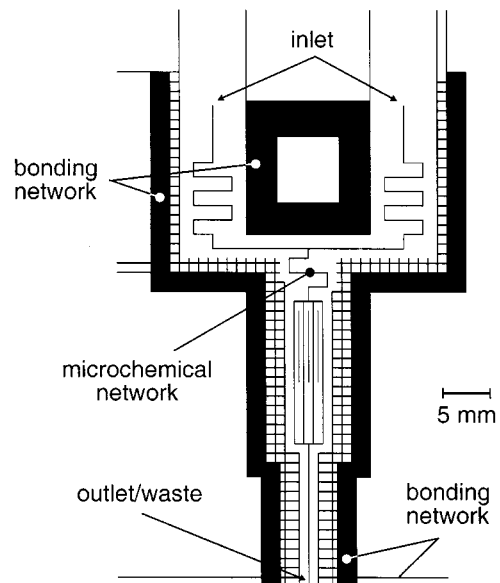


Fig. 4. Mask pattern for the wet etching of a microchemical device. Black regions are openings in the chromium layer and thus etched regions. Network lines are 10 μm wide. Two microchemical devices are laid out on each wafer.

<sup>5</sup>Clariant AG, Muttens, Switzerland.

<sup>6</sup>Alliance Recording HN, Agfa-Gevaert, Belgium.

<sup>7</sup>Schott, Germany.

surfaces are polished to a “three diamond” finish, which means that the arithmetic average deviation of the absolute values of the roughness profile from the mean line ( $R_a$ ) is better than or equal to 20 Å.

### B. Glass Substrate Bonding

Microfluidics and cover wafers are bonded together by means of two different methods. Systems with an intermediate Al aperture layer are anodically bonded [27], [29]; the systems without such a layer are thermally bonded [23], [24]. As experienced with the first version of the chip (with partially integrated optical elements), wafer surfaces must be perfectly clean and free of dust particles in order to get homogenous bonding. Moreover, air bubbles may remain trapped between the wafers, preventing a perfect bonding. If unbonded spots are located in the microfluidic network region, they cause leakage. These are the reasons why the wafers are cleaned in a class 100 atmosphere and why (Fig. 4) a second microchannel grid is patterned around the chemical microfluidic network. This grid reduces the surface to be bonded and therefore the probability to have unbonded zones around the chemical microfluidic network. Since this grid pattern is connected with the outside atmosphere, it also enables trapped air and gases to escape from hot wafers during the bonding process [24]. Fig. 5(a) shows the setup for thermal bonding. The cover wafer is first placed manually (using tweezers) on the etched wafer, so that the access holes align with the ends of the channels. The stacked system is then placed between two 2-mm-thick ceramic plates and transported outside the cleanroom to a furnace.<sup>8</sup> To ensure good contact between the wafers, a metal cylinder ( $\sim 1$  kg) is placed on top of the stack. Some chips were bonded with two 0.5-mm-thick nonwoven alumina/silica fabrics<sup>9</sup> placed between the wafers and the ceramic plates [Fig. 5(a)]. This soft layer ensures better pressure distribution. The bonding temperature profile is given in Fig. 6. This bonding cycle is repeated once or twice with weights of  $\sim 150$  g placed over unbonded or poorly bonded regions, as evidenced by whitish or slightly opaque regions or interference fringes. Fig. 5(b) presents the setup for anodic bonding. The glass wafers are aligned under the microscope (with the help of alignment marks) and then placed on the hot plate of the bonding setup. A single-sided polished silicon wafer is placed on top of the chip. The rough side of the silicon wafer is placed in contact with the glass surface to prevent the silicon wafer and glass wafer from bonding. This conductive wafer enables a homogeneous electric field distribution. The electrodes (three metallic feet fixed on an aluminum plate and weighing  $\sim 150$  g) are then lowered onto the stacked wafers. The system is heated up from ambient cleanroom temperature to 450 °C in 15 min. The voltage between the hot plate and the electrodes is then increased (with a current limitation of 4 mA) from 0 to 0.7–0.8 kV. The temperature and potential are kept constant for  $\sim 15$  min as the current slowly decreases to  $\sim 2.6$  mA. The potential and the hot plate are then switched off. The system is left on the hot plate and cooled down from 450 °C to room temperature.

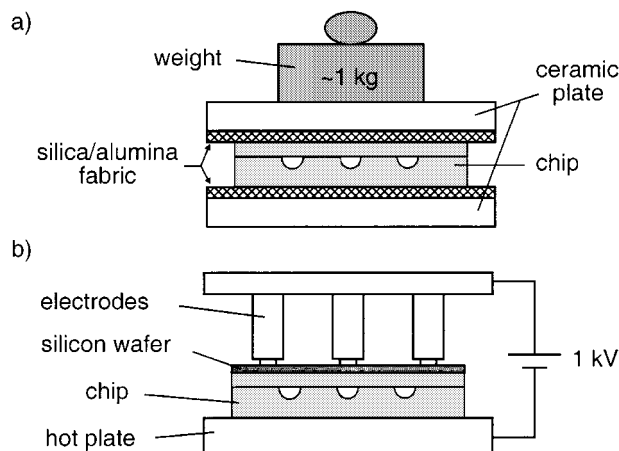


Fig. 5. Bonding setups. (a) For thermal bonding and (b) for anodic bonding.

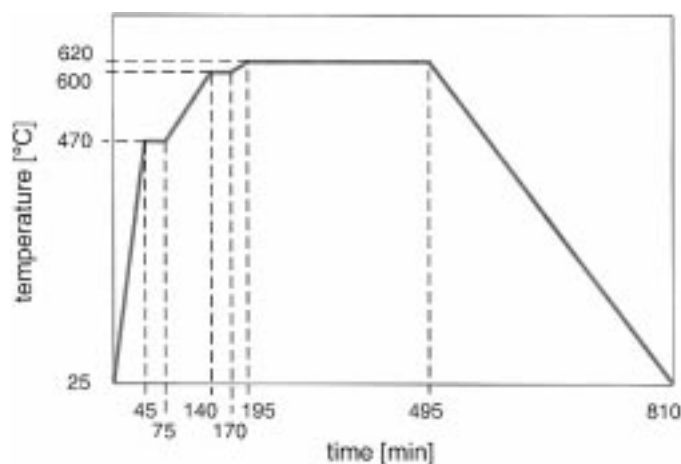


Fig. 6. Thermal bonding temperature profile.

## III. DETECTION SYSTEM

### A. Aperture Arrays

Before the formation of integrated aperture and microlens array layers, the inlets of the microfluidic chip are sealed up with small 5 mm squares of polyimide-silicone adhesive tape.<sup>10</sup> This prevents contamination of the microchannels by solvent and photoresist developer, or clogging with photoresist. As shown in point 3 of Fig. 3, the detection system process begins with an LPCVD deposition of a 2000-Å chromium layer on both sides of the chemical chip. These layers are successively patterned by means of the same technique described in Section II-A (wet etching), except that the KOH etchant is replaced by a chromium-etching solution (100 g of  $\text{Ce}(\text{SO}_4)_2 \cdot 4\text{H}_2\text{O}$ , 135 g of  $(\text{NH}_4)_2\text{Ce}(\text{NO}_3)_6$ , and 50 mL of  $\text{H}_2\text{SO}_4$  in 1000 mL of  $\text{H}_2\text{O}$ ). The etching time is  $\sim 15$  min at room temperature ( $\sim 21$  °C). To enable efficient collection of the fluorescence light as well as efficient separation between the excitation beam and the fluorescent light, the various elements making up the detection system (aperture and microlens arrays) must be aligned within a  $\sim 5$   $\mu\text{m}$  range with respect to the microchannels. Special alignment marks on the photolithographic mask allow precise positioning of the first chromium aperture array with respect to the

<sup>8</sup>Heraeus Instruments M110, Hanau, Germany.

<sup>9</sup>Goodfellow Cambridge Ltd, Cambridge, U.K.

<sup>10</sup>3M, Austin, TX.

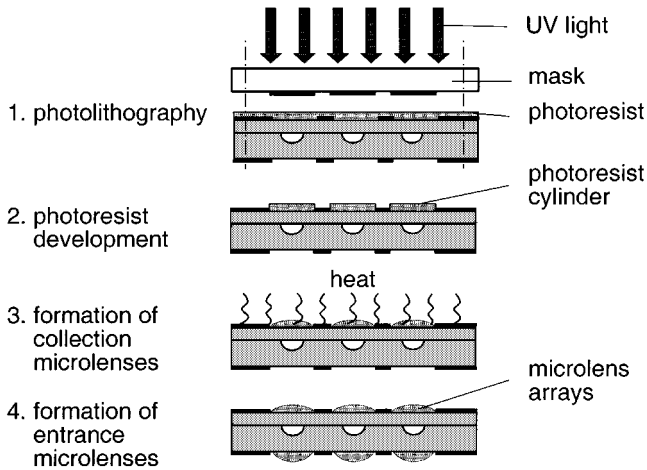


Fig. 7. Refractive microlens deposition. The focal length of the entrance (excitation) and exit (collection) microlenses are  $\sim 1.4$  mm and  $\sim 2.0$  mm, respectively.

etched microchannels ( $< 4 \mu\text{m}$ ). Alignment marks are also etched into this first chromium layer to allow later alignment (within  $< 2 \mu\text{m}$ ) of the second chromium aperture array, and, in turn, the two microlens arrays. The overall alignment tolerances between the sealed microchannels and the second aperture and microlens arrays is  $< 6 \mu\text{m}$ .

### B. Microlens Arrays

As shown in (1) and (2), a good SNR is directly related to large fluorescence signal  $\bar{S}_F$  and to small background signal  $\bar{S}_B$ . Defects (scratches) on microlenses used to focus the excitation beam can scatter part of the excitation beam, reducing the amount of light usable for fluorochrome excitation and hence  $\bar{S}_F$ , while increasing the background signal  $\bar{S}_B$ . Defects on microlenses used to collect the fluorescence light reduce only the amount of fluorescence light reaching the photodetector and hence reduce only slightly  $\bar{S}_F$  (the size of the fluorescence spot is small compared to the active area of the photodetector). Therefore, the surface quality of microlenses used to focus the excitation beam into the microchannel is more important than the surface quality of the microlenses used for fluorescence light collection. The illumination microlenses are deposited after the collection microlenses in order to reduce the risk of microlens surface deterioration during deposition of the second array of microlenses. Fig. 7 shows the microlens array fabrication steps. A  $30\text{-}\mu\text{m}$ -thick layer of AZ4562 photoresist<sup>11</sup> is deposited on the side of the chip with the inlet holes. The photoresist is deposited using an RC8THT spin-coater coupled with an ACS hot plate.<sup>12</sup> After the photoresist deposition, the wafers are directly and automatically transported to the hot plate for 4-min soft-baking at  $110^\circ\text{C}$ . An MA8-BA6 mask aligner<sup>13</sup> is used to expose and pattern the photoresist. An AZ400K is used as a developer. The rinsed and dried wafers are finally placed, photoresist structures up, at  $0.5$  mm above the ACS hot plate ( $150^\circ\text{C}$ , 2 min). The heated photoresist cylinders melt, and under the influence of the surface tension, microlenses are formed. The mi-

TABLE I  
ETCHING RATE AND MICROFLUIDIC DEPTHS

batch number	etching rate	average microfluidic depth
1	$1.2 \mu\text{m}/\text{min}$	$24.0 \mu\text{m}$
2	$1.1 \mu\text{m}/\text{min}$	$24.4 \mu\text{m}$
3	$1.0 \mu\text{m}/\text{min}$	$24.8 \mu\text{m}$
4	$0.9 \mu\text{m}/\text{min}$	$24.7 \mu\text{m}$

crochannels for the focusing of the excitation light are deposited in the same way on the other side of the chip. The only difference lays in the photoresist thickness, which is  $16.5 \mu\text{m}$  instead of  $30 \mu\text{m}$  (a thinner photoresist layer leads to a thinner microlens and thus to a longer focal length). A  $70\text{-}\mu\text{m}$  PVC adhesive film is used to protect the first microlens array during the second deposition. The film is removed just before the melting procedure.

Circular and elliptical microlenses are obtained by melting photoresist cylinders having circular and elliptical bases, respectively. The base shape is given by the pattern on the chromium photolithographic mask. Square, hexagonal, or even ring-shaped microlenses are also possible [21].

## IV. RESULTS AND DISCUSSIONS

Small ( $10 \times 10 \text{ mm}^2$ ) wafer pieces were used to evaluate the roughness of the etched surfaces. These glass samples were etched to a depth of  $\sim 25 \mu\text{m}$  in 20% HF, and the surface roughness was measured with an Alpha Step 500 profilometer<sup>14</sup> equipped with a  $12.5\text{-}\mu\text{m}$  stylus. The Ra of Pyrex glass samples after wet etching is smaller than  $21 \text{ \AA}$  (Ra  $< 13 \text{ \AA}$  before etching). Though the surface roughness increased, it remained close to the “three diamond” limit (Ra  $< 20 \text{ \AA}$ ). Half-spherical cavities with a radius ranging from a few micrometers to a few tens of micrometers were also visible after etching. It is likely that microbubbles, inclusions, or local chemical modifications [30] were at the root of these cavities. These were few in number and did not cause any problems for the etching of the microfluidic network. These tests also showed that the etching rate is strongly dependent on the acid temperature [30] and on the number of wafers already etched. This is why the etching process was performed in two steps: a first step to determine the etching rate (etching time of  $\sim 20$  min) and a second step to adjust the microchannel depths. The microchannel depths were measured with a profilometer at six places spread equally over the wafer. Table I shows the etching rate of four batches (total of eight wafers) made in the same acid bath. The etching rate was between  $1.2$  (first batch, freshest acid bath) and  $0.9$  (fourth batch)  $\mu\text{m}/\text{min}$ . The relative difference between the average microchannel depths achieved and the nominal depth is 4% or better. The standard deviation of the microchannel depths within the same batch is smaller than  $0.6 \mu\text{m}$ . Fig. 8 shows a cross-sectional view of a microchannel. Since the wet-etching process with HF is isotropic, the microchannel section consists of a half-circle with a flat bottom. The width of the flat bottom is

<sup>11</sup>Clariant AG, Muttenz, Switzerland.

<sup>12</sup>Karl Süß, Garching/Munich, Germany.

<sup>13</sup>Karl Süß, Garching/Munich, Germany.

<sup>14</sup>Tencor Instruments, Mountain View, CA.

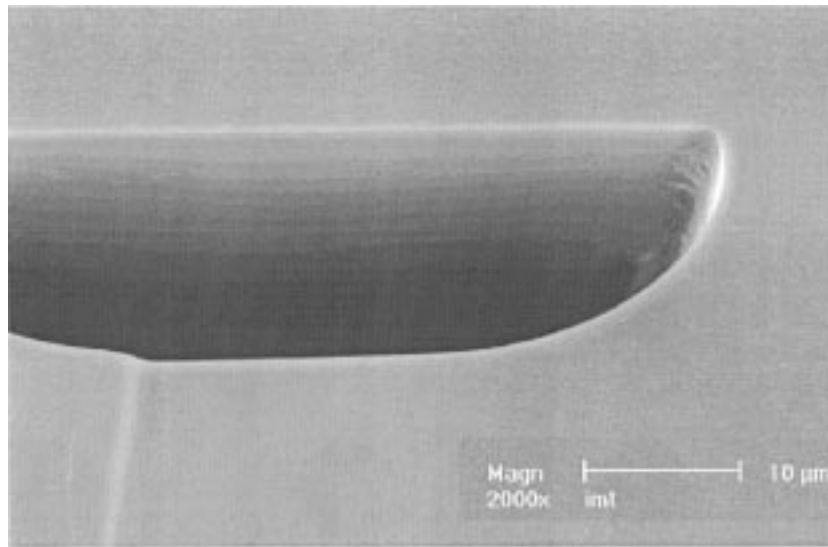


Fig. 8. Scanning electron micrograph (SEM) of a cross-sectional view of a microchannel.

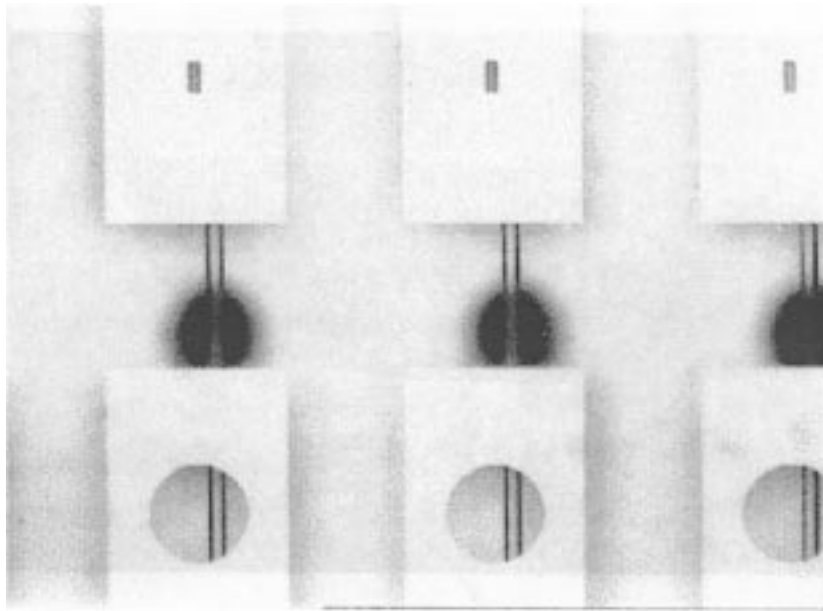


Fig. 9. Intermediate aperture layer deposited along parallel microfluidic channels. The slightly defocused dark circles are the apertures in the layer deposited on the bottom surface (excitation side) of the chip.

given by the mask opening ( $10\ \mu\text{m}$  wide), and the radius of the side walls (etched distance under the poly-Si mask) is equal to the microchannel depth and hence proportional to the etching time.

For the first chip design (without the additional microchannel grid to help the bonding), about three thermal bonding cycles were necessary on average to get sealed microfluidic networks [19]. This is time consuming, since one bonding cycle requires  $\sim 13\ \text{h}$  (Fig. 6). The new chip design enabled the reduction of the number of cycles to about two. One cycle was sufficient for the chips bonded with the alumina/silica fabric. As described in Section II-B, the second and third bonding cycles were executed with small weights placed over poorly bonded regions. The weights produced marks on the chip surface, which reduced the regularity and the accuracy of the thickness of the photoresist layer deposited for the fabrication of the microlenses. The microlens quality (accuracy of focal length, profile control)

is hence reduced. Moreover, the marks on the surface cause scattering of the excitation beam, which increases the SNR. The thermal bonding with the alumina/silica fabric reduced the bonding time and increased the surface quality of the chip even though the nonwoven fabric also slightly marked the glass. Chips bonded with the alumina/silica fabric were perfectly sealed without any unbonded regions, and, as shown in Fig. 8, there is no visible interface between the wafers.

Anodic bonding required only one cycle to seal microfluidic networks. This process is faster (cycle of  $\sim 45\ \text{min}$ ) than the thermal bonding process (cycle of  $\sim 13\ \text{h}$ ) and enables the bonding of two glass wafers with an intermediate aperture layer if needed. On the other hand, the process requires a  $\text{Si}_3\text{N}_4$  layer deposition. Fig. 9 shows the two kinds of intermediate apertures that were integrated: 1) a rectangular aperture with the same width as the microchannel and 2) a circular aperture larger than

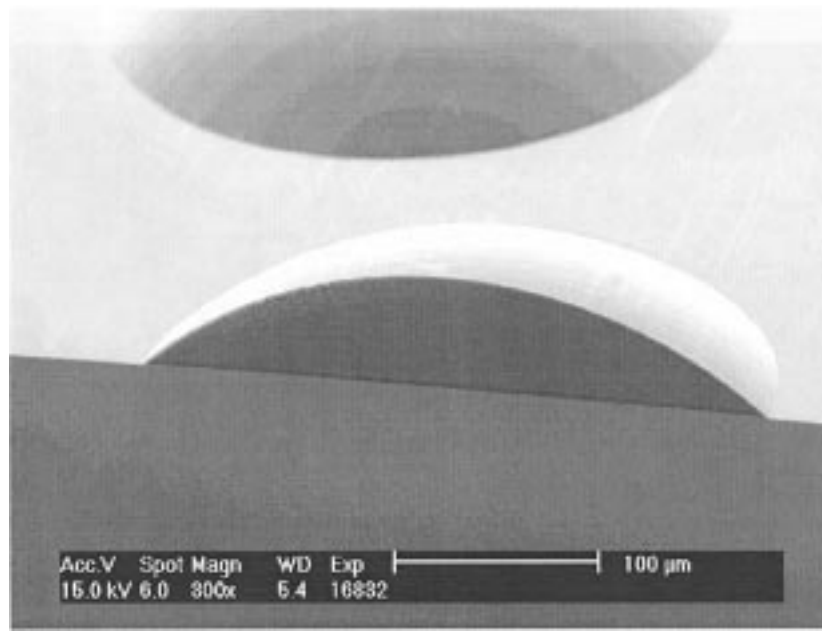


Fig. 10. Section of a 310- $\mu\text{m}$ -wide photoresist microlens.

the microchannel width. One can also see the microchannels passing under the apertures and the slightly defocused dark circles, which are the apertures in the layer deposited on the bottom surface (excitation side) of the chip. The circular apertures are less efficient than the rectangular ones (they do not block all the light that is not focused into the microchannel), but they are more tolerant to misalignment. This can be seen in Fig. 9, where the apertures are not perfectly aligned with respect to the microchannels (shifted by  $\sim 60 \mu\text{m}$  to the left). The circular apertures are still operational, whereas the rectangular ones block the microchannel and the fluorescence light completely. The misalignment was due to the very simple setup used for anodic bonding, which did not allow monitoring or to modification of the wafer alignment when the electrodes were lowered. The different feet did not touch the silicon wafer exactly at the same moment, which caused a slight displacement of the stacked wafers. Printed film was used as the photolithographic mask, which did work well. However, precise alignment was difficult to achieve since the taped film sometimes rubbed against the photoresist. Moreover, when the wafer was placed within proximity of the mask for exposition, the film tended to shift slightly. This technique is cheap and useful for systems with simple and low-resolution structures, but it is not suitable when precise alignment ( $< \pm 20 \mu\text{m}$ ) for a multimask process is required.

Fig. 10 shows an SEM picture of a cut photoresist microlens. In this system, two kinds of refractive microlenses were deposited to focus the excitation beam into the microchannel: a 350- $\mu\text{m}$ -wide and 25- $\mu\text{m}$ -high circular microlens and a 350  $\times$  400  $\mu\text{m}$ -wide and 27- $\mu\text{m}$ -high elliptical one. The microlens quality on both sides of the chip was tested with the help of a Twyman–Green interferometer [31]. The standard deviation  $\sigma_w$  of the microlens surface profiles from an ideal sphere is, in both cases,  $\sigma_w = 0.11 \lambda$ . This corresponds to a Strehl ratio of  $\sim 0.76$  [32]. Even if the microlenses are not diffraction-limited (an optical system is considered diffraction-limited when the Strehl ratio is  $\geq 0.8$ ), the microlens quality is sufficient for

nonimaging systems. Moreover, the collection side microlenses deposited first were not damaged or affected by the fabrication of the excitation side microlenses. Microlenses of equal quality can hence be directly deposited on both sides of the same substrate in two subsequent fabrication steps. The reproducibility in the microlens focal lengths is within 2%.

Fig. 11 shows the complete system as seen from the collection side. Several collection microlenses were deposited along each sealed microchannel. The pitch between the parallel microchannels is 1 mm but could be reduced to 360  $\mu\text{m}$  since the minimum pitch is given by the bigger microlens diameter plus a gap of  $\sim 10 \mu\text{m}$  necessary for microlens fabrication. Fig. 12 shows the fluorescence spot in the microfluidic channel filled with a solution containing fluorescent dye when the excitation beam is focused by (a) a circular microlens and (b) an elliptical microlens. The elliptical microlens has smaller aberrations for off-axis excitation and gives therefore a better focused spot, which leads to a higher excitation intensity and enables easier and more efficient fluorescent light collection. Fig. 13 shows the average signals obtained when Cy5 solutions in phosphate buffer (pH 7.4) having concentrations ranging from 1 nM to 50  $\mu\text{M}$  were pumped through the microfluidic network. The excitation beam was focused with elliptical and circular microlenses, respectively. The signals obtained for the buffer solution are presented as horizontal lines. The absolute values of the average signal obtained with the elliptical excitation microlens ( $\overline{S}_E$  and  $\overline{S}_{BE}$ ) were greater than the signals obtained with the circular microlens ( $\overline{S}_C$  and  $\overline{S}_{BC}$ ). On average,  $\overline{S}_E$  is 15% greater than  $\overline{S}_C$ , whereas, for the buffer solution,  $\overline{S}_{BE}$  is 9% greater than  $\overline{S}_{BC}$ . Since the size of the elliptical excitation microlens is 13% greater than the circular excitation microlens, a signal difference of this magnitude was expected. The better excitation spot shape obtained with the elliptical microlens [Fig. 12(b)] explains why the signal difference is more significant for the microchannels filled with Cy5 solution ( $\overline{S}_E - \overline{S}_C$ ) than for the microchannels

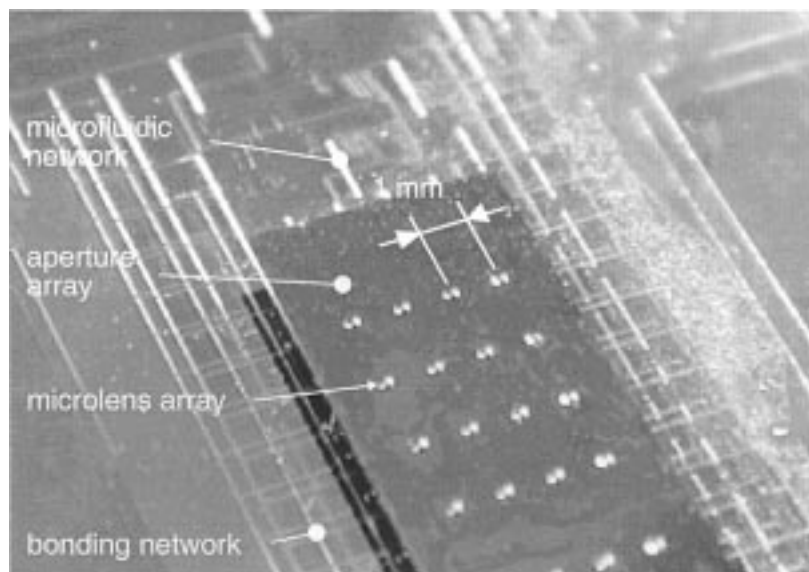


Fig. 11. View on the collection side of the microchemical system. One can see the 260- $\mu\text{m}$ -wide 49- $\mu\text{m}$ -high microlens array deposited onto the aperture array. Unlike the excitation side aperture array, which is deposited on the whole wafer surface, the collection-side aperture array is limited to a zone of  $5 \times 16 \text{ mm}^2$ , which allows the flow inside the microchannels to be observed. The microfluidic and bonding networks, as well as their mirror image on the excitation side aperture array, are also visible.

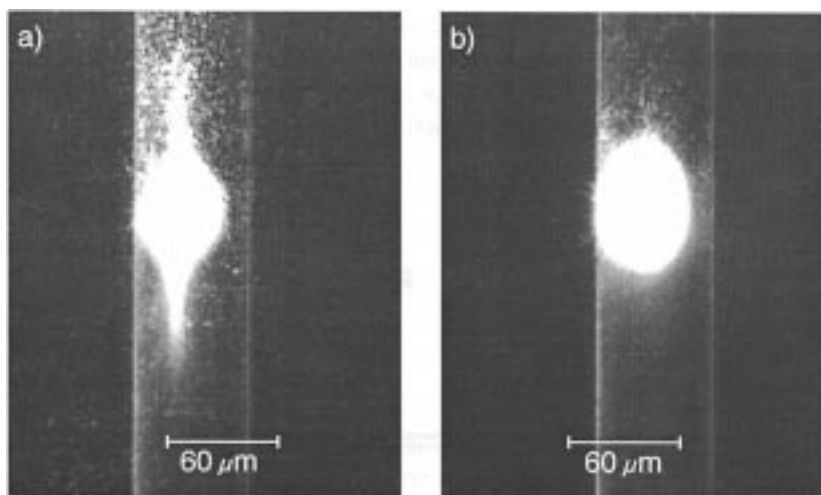


Fig. 12. Fluorescence spots in a microfluidic channel when the light is focused by (a) a circular microlens and (b) an elliptical microlens.

filled with plain buffer solution ( $\bar{S}_{BE} - \bar{S}_{BC}$ ). Therefore, the elliptical microlens, beside enabling a slightly larger excitation power to be coupled into the microchemical chip, improves slightly the signal difference when the microchannels are filled with Cy5 solution versus buffer solution, and hence improves the SNR. Fig. 14 shows the signal obtained when DI water (signal equivalent to the signal obtained for phosphate buffer solution) and 10-nM Cy5 solution (in phosphate buffer pH 7.4) were pumped through the microchannel. The excitation was provided by a 5-mW He-Ne laser giving an excitation power in the microchannel of  $0.24 \pm 0.02 \text{ mW}$ . The collected fluorescence light was collimated through an 800- $\mu\text{m}$  pinhole placed 2 mm away from the chip onto a photomultiplier tube.<sup>15</sup> According to the data sheet, the electronic bandwidth of the photomultiplier output signal is 20 kHz. The signal was filtered

by means of an XF46 EM interference filter<sup>16</sup> placed in front of the photomultiplier. The acquisition of the photomultiplier signal was realized on a PC, equipped with a PCI-MIO-16E-4 data-acquisition card and LabVIEW.<sup>17</sup> The sampling frequency was 10 Hz (ten samples per second).

The photobleaching phenomenon (destruction of fluorescence dye molecules) is clearly visible when the liquid flow is stopped after 60 s; the signal emitted by the Cy5 solution decreases by  $\sim 30\%$ . Compared to the system with partially integrated optical elements described in the introduction [19], the sensitivity has been improved by about a factor of three, and the LOD of the fully integrated detection system (excitation beam focused by an elliptical microlense) is 3.3 nM (SNR = 9).

<sup>15</sup>Hamamatsu H5701-5.

<sup>16</sup>Omega Optical Inc, Brattleboro, VT.

<sup>17</sup>National Instruments Corporation, Austin, TX.

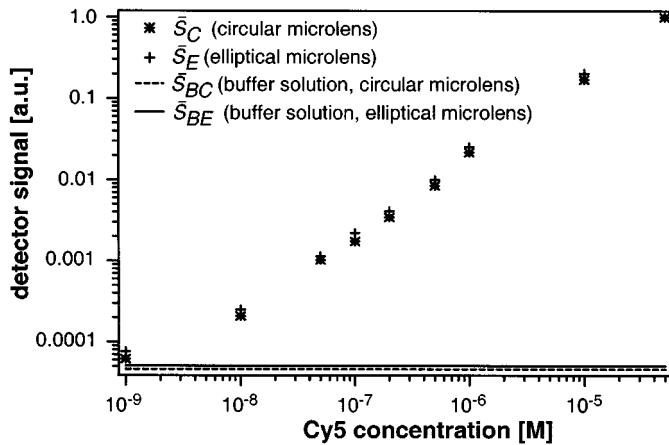


Fig. 13. Log-log plot of the fluorescence signal recorded when the excitation beam was focused by a circular or an elliptical microlens. The excitation power was  $0.24 \pm 0.02$  mW.

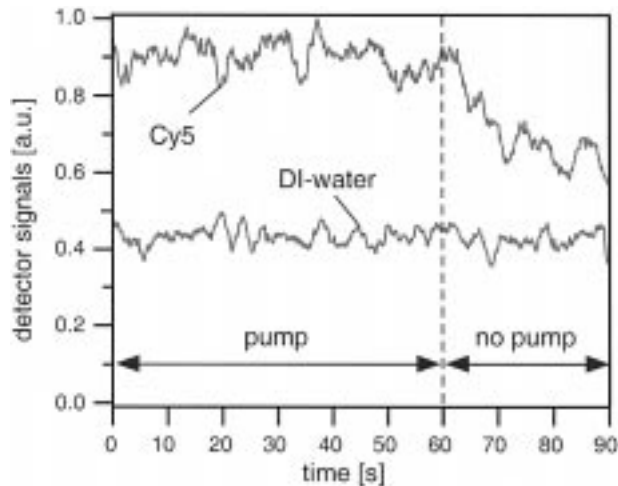


Fig. 14. Signal detected for a 10-nM Cy5 solution and DI water pumped through the microfluidic channel. All data were smoothed using a 21-point box smooth algorithm, implemented in Igor Pro (Wavemetrics, Lake Oswego, OR).

## V. CONCLUSION

Microfabrication enables the integration of microlens arrays and aperture arrays directly onto and within microchemical chips. As shown previously, fluorescence signals emitted from dye solutions with concentrations on the order of few nM can be recorded. The optimization of the design and the improvement of fabrication techniques should yield sensitivities of a few hundred pM and even achieve sensitivities comparable to those obtained with standard detection systems [10]. The microfabrication techniques used for the chemical chip and the integration of the detection system enable precise alignment of the optical elements with respect to the microfluidics, as well as the fabrication of chemical systems with closely spaced microfluidic channels and detection systems. Integrating the excitation sources (light-emitting diodes, laser diodes, or vertical-cavity surface-emitting lasers) and the detectors will permit the realization of compact high throughput  $\mu$ TAS.

This technology can also be used to realize stacked optical systems combining refractive and diffractive optical elements and aperture arrays for a wide range of applications such as

integrated spectrometers [33], imaging systems for photolithography [21], or coupling light into optical fibers [34]. Moreover, the optical elements deposited onto Pyrex wafers can be bonded onto micromachined silicon wafers to realize a wide range of microoptoelectromechanical systems (MOEMS).

## ACKNOWLEDGMENT

The authors would like to thank C. Ossman, M. Heisner (Karl Süss, Neuchâtel), and K. Weible (Weible Optech, Neuchâtel) for their help in microlens fabrication and measurements; G. Mondin and S. Jeanneret [Sensors, Actuators, Microsystem Laboratory (SAMPLAB), IMT, Neuchâtel] for the metallic layer depositions; A. Dodge (SAMPLAB, IMT, Neuchâtel) for his work in glass wet etching; and J. Lichtenberg (SAMPLAB, IMT, Neuchâtel) for technical support and helpful discussions.

## REFERENCES

- [1] E. Verpoorte, A. Manz, H. Lüdi, A. E. Bruno, F. Maystre, B. Krattiger, H. M. Widmer, B. H. van der Schoot, and N. F. de Rooij, "A silicon flow cell for optical detection in miniaturized total analysis systems," *Sens. Actuators B, Chem.*, vol. 6, pp. 66–70, 1992.
- [2] Z. Liang, N. Chiem, G. Ocvirk, T. Tang, K. Fluri, and D. J. Harrison, "Microfabrication of a planar absorbance and fluorescence cell for integrated capillary electrophoresis devices," *Anal. Chem.*, vol. 68, pp. 1040–1046, 1996.
- [3] H. Salimi-Moosavi, Y. Jiang, L. Lester, G. McKinnon, and D. J. Harrison, "A multireflection cell for enhanced absorbance detection in microchip-based capillary electrophoresis devices," *Electrophoresis*, vol. 21, pp. 1291–1299, 2000.
- [4] N. Burggraf, B. Krattiger, A. J. de Mello, N. F. de Rooij, and A. Manz, "Holographic refractive index detector for application in microchip-based separation systems," *Analyst*, vol. 123, pp. 1443–1447, 1998.
- [5] K. Swinney, D. Markov, and D. J. Bornhop, "Chip-scale universal detection based on backscatter interferometry," *Anal. Chem.*, vol. 72, no. 13, pp. 2690–2695, 2000.
- [6] A. T. Woolley, G. F. Sensabaugh, and R. A. Mathies, "High-speed DNA genotyping using microfabricated capillary array electrophoresis chips," *Anal. Chem.*, vol. 69, pp. 2181–2186, 1997.
- [7] J. S. Rossier, M. A. Roberts, R. Ferrigno, and H. H. Girault, "Electrochemical detection in polymer microchannels," *Anal. Chem.*, vol. 71, pp. 4294–4299, 1999.
- [8] R. S. Martin, A. J. Gawron, and S. M. Lunte, "Dual-electrode electrochemical detection for poly(dimethylsiloxane)-fabricated capillary electrophoresis microchips," *Anal. Chem.*, vol. 72, pp. 3196–3202, 2000.
- [9] G. Ocvirk, T. Tang, and D. J. Harrison, "Optimization of confocal epifluorescence microscopy for microchip-based miniaturized total analysis systems," *Analyst*, vol. 123, pp. 1429–1434, 1998.
- [10] G. Jiang, S. Attiya, G. Ocvirk, W. E. Lee, and D. J. Harrison, "Red diode laser induced fluorescence detection with a confocal microscope on a microchip for capillary electrophoresis," *Biosens. Bioelectron.*, vol. 14, pp. 861–869, 2000.
- [11] A. Manz, N. Graber, and H. M. Widmer, "Miniaturized total chemical analysis systems: a novel concept for chemical sensing," *Sens. Actuators B, Chem.*, vol. 1, pp. 244–248, 1990.
- [12] J. C. Fister III, S. C. Jacobson, L. M. Davis, and J. M. Ramsey, "Counting single chromophore molecules for ultrasensitive analysis and separations on microchip devices," *Anal. Chem.*, vol. 70, pp. 431–437, 1998.
- [13] B. B. Haab and R. A. Mathies, "Single-molecule detection of DNA separations in microfabricated capillary electrophoresis chips employing focused molecular streams," *Anal. Chem.*, vol. 71, pp. 5137–5145, 1999.
- [14] I. Kheterpal and R. A. Mathies, "Capillary array electrophoresis," *Anal. Chem.*, pp. 31A–36A, 1999.
- [15] V. P. Jaecklin, C. Linder, N. F. de Rooij, J.-M. Moret, and R. Vuilleumier, "Line-addressable torsional micromirrors for light modulator arrays," *Sens. Actuators A, Phys.*, vol. 41, pp. 324–329, 1994.
- [16] M. C. Wu, "Micromachining for optical and optoelectronic systems," *Proc. IEEE*, vol. 85, pp. 1833–1855, 1997.
- [17] J.-C. Roulet, K. Fluri, E. Verpoorte, R. Völkel, H. P. Herzig, N. F. de Rooij, and R. Dändliker, "Micro-optical systems for fluorescence detection in  $\mu$ TAS applications," in *Micro Total Analysis Systems '98*, D. J. Harrison and A. van den Berg, Eds. Banff, Canada: Kluwer Academic, 1998, pp. 287–290.

- [18] J.-C. Roulet, E. Verpoorte, R. Völkel, H. P. Herzig, N. F. de Rooij, and R. Dändliker, "Microlens systems for fluorescence detection in chemical microsystems," *Opt. Eng.*, vol. 40, no. 5, 2001.
- [19] J.-C. Roulet, K. Fluri, E. Verpoorte, R. Völkel, H. P. Herzig, N. F. de Rooij, and R. Dändliker, "Micro-optic integration for fluorescence detection in  $\mu$ TAS systems," in *Transducers'99*, vol. 1, Sendai, Japan, 1999, pp. 120–123.
- [20] H. P. Herzig, Ed., *Micro-optics, Elements, Systems and Applications*. London, U.K.: Taylor & Francis, 1997.
- [21] P. Nussbaum, R. Völkel, H. P. Herzig, M. Eisner, and S. Haselbeck, "Design, fabrication and testing of microlens arrays for sensors and microsystems," *Pure Appl. Opt.*, vol. 6, pp. 1–20, 1997.
- [22] A. Dogdage, K. Fluri, V. Linder, G.-L. Lettieri, J. Lichtenberg, E. Verpoorte, and N. F. de Rooij, "Valveless, sealed microfluidics device for automated heterogeneous immunoassay: design and operational considerations," in *Micro Total Analysis Systems 2000*, A. van den Berg, W. Olthuis, and P. Bergveld, Eds. Enschede, The Netherlands: Kluwer Academic, 2000, pp. 407–410.
- [23] Z. Fan and D. J. Harrison, "Rapid injection and separation of amino acids with capillary electrophoresis systems micromachined on a glass chip," *Anal. Chem.*, vol. 66, pp. 177–184, 1994.
- [24] M. Stjernström and J. Roeraade, "Method for fabrication of microfluidic systems in glass," *J. Micromech. Microeng.*, vol. 8, pp. 33–38, 1998.
- [25] G. R. Bright and D. L. Taylor, "Imaging at low light level in fluorescence microscopy," in *Application of Fluorescence in the Biomedical Sciences*, D. L. Taylor, Ed. New York: Liss, 1986, pp. 257–288.
- [26] H. K. Pulker, *Coatings on Glass*, Amsterdam, The Netherlands: Elsevier, 1984.
- [27] A. Berthold, L. Nicola, P. M. Sarro, and M. J. Vellekoop, "Glass-to-glass anodic bonding with standard IC technology thin films as intermediate layers," *Sens. Actuators A, Phys.*, vol. 82, pp. 224–228, 2000.
- [28] G. T. A. Kovacs, *Micromachined Transducers Sourcebook*. New York: WCB McGraw-Hill, 1998.
- [29] M. Nese and A. Hanneborg, "Anodic bonding of silicon to silicon wafers coated with aluminum, silicon oxide, polysilicon or silicon nitride," *Sens. Actuators A, Phys.*, vol. 37, pp. 61–67, 1993.
- [30] G. A. C. Spierings and J. van Dijk, "The dissolution of  $\text{Na}_2\text{O}-\text{MgO}-\text{SiO}_2$  glass in aqueous HF solutions," *J. Mater. Sci.*, vol. 22, pp. 1869–1874, 1987.
- [31] J. Schwider and O. Falkenstörfer, "Twyman-Green interferometer for testing microspheres," *Opt. Eng.*, vol. 34, no. 10, pp. 2972–2975, 1995.
- [32] D. Malacara and Z. Malacara, "Handbook of lens design," in *Opt. Eng.*. New York: Marcel Dekker, 1994.
- [33] S. Traut and H. P. Herzig, "Holographically recorded gratings on microlenses for a miniaturized spectrometer array," *Opt. Eng.*, vol. 39, no. 1, pp. 290–298, 2000.
- [34] R. Göring *et al.*, "Miniaturized piezoelectrically driven fiber optics switches with transmissive microoptics," in *Proc. SPIE Miniaturized Systems with Micro-Optics and MEMS*, vol. 3878, Santa Clara, CA, 1999, pp. 136–143.

**Jean-Christophe Roulet** received the diploma in electrical and electronic engineering from the Swiss Technical College, Le Locle, Switzerland, in 1989 and the engineering degree in microtechnology from the Swiss Federal Institute of Technology, Lausanne, Switzerland, in 1995. He received the Ph.D. degree in optics from the Institute of Microtechnology, University of Neuchâtel, Switzerland, in 2001.

From June 1995 to February 1996, he was with the Development Department of ASCOM Tech., Berne, Switzerland. In 1996, he became a graduate student with the Applied Optics Group at the Institute of Microtechnology, University of Neuchâtel, working in the field of optical systems applied to integrated chemical sensor applications ( $\mu$ TAS).

**Reinhard Völkel** received the diploma in physics and the Ph.D. degree from the University of Erlangen-Nuernberg, Germany, in 1989 and 1994, respectively.

He worked on diffractive optical elements for optical interconnects. He joined the Institute of Microtechnique at the University of Neuchâtel, Switzerland, in 1994, where he worked on microoptics, imaging systems, photolithography, and biosensors. Since 1999, he has been in charge of the Micro-Optics Department of Karl Süss KG, Neuchâtel, Switzerland. He is involved in the development and fabrication of refractive microlens arrays for imaging and illumination purposes within photolithography systems.

**Hans Peter Herzig** received the diploma in physics from the Swiss Federal Institute of Technology, Zürich, Switzerland, in 1978 and the Ph.D. degree in optics from the University of Neuchâtel, Switzerland, in 1987.

From 1978 to 1982, he was a Scientist with the Optics Development Department of Kern, Aarau, Switzerland, working in lens design and optical testing. In 1983, he became a Graduate Research Assistant with the Applied Optics Group, Institute of Microtechnology, University of Neuchâtel, working in the field of holographic optical elements, especially scanning elements. He currently heads the microoptics research group and is an Associate Professor at the University of Neuchâtel.

Dr. Herzig is a member of the Optical Society of America (OSA) and EOS and a board member of the Swiss Society of Optics and Microscopy.

**Elisabeth Verpoorte** received the Ph.D. degree in analytical chemistry from the University of Alberta, Edmonton, AB, Canada, in 1990.

The subject of her dissertation was concerned with the use of ac impedance analysis for studying the permeability and behavior of dissociable species in PVC-based ion-selective membranes. She held a postdoctoral position and, later, a permanent position as a Research Scientist in the Corporate Analytical Research Department of Ciba Ltd., Basel, Switzerland, working on the development of miniaturized total analysis systems ( $\mu$ TAS). In July 1996, she became Team Leader in the group of Prof. N. F. de Rooij at the Institute of Microtechnology, University of Neuchâtel, Switzerland, where her research interests continue to concentrate in the area of  $\mu$ TAS for bioanalytical applications.

**Nico F. de Rooij** (M'84–SM'00) joined the Institute of Microtechnology, University of Neuchâtel, Switzerland (IMT UNI-NE), as Professor and Head of the Sensors, Actuators and Microsystems Laboratory in 1982. From October 1990 to October 1996, he was Director of IMT UNI-NE. He lectured at the Swiss Federal Institute of Technology, Zurich, Switzerland. Since 1989, he has been a part-time Professor at the Swiss Federal Institute of Technology, Lausanne. His research activities include microfabricated sensors, actuators, and microsystems. He was a Member of the Steering Committee of the International Conference on Solid-State Sensors and Actuators and of Eurosensors. He was European Program Chairman of Transducers '87 and General Chairman of Transducers '89. He is a member of the editorial boards of *Sensors and Actuators* and *Sensors and Materials*.

Dr. de Rooij is a member of the Editorial Board of the JOURNAL OF MICROELECTROMECHANICAL SYSTEMS.

**René Dändliker** received the diploma in physics from the Swiss Federal Institute of Technology, Zurich, in 1963, the Ph.D. degree in physics from the University of Berne, Switzerland, in 1968, and the *Venia Legendi* degree in applied physics from the Swiss Federal Institute of Technology in 1978.

From 1963 to 1969, he was a Graduate Research Assistant with the Institute of Applied Physics, University of Berne, working on gas and solid-state lasers. From 1969 to 1970, he was a Research Scientist with the Philips Research Laboratories, Eindhoven, the Netherlands, working in the field of applied optics. From 1970 to 1978, he was a Senior Scientist and Head of the Coherent Optics Group at the Brown Boveri Research Center, Baden, Switzerland, where he was concerned with optical metrology applied to mechanics, such as laser Doppler velocimetry and heterodyne holographic interferometry. Since 1978, he has been a Professor of applied optics with the University of Neuchâtel, Switzerland, and since 1989 also a Professor of applied optics with the Swiss Federal Institute of Technology, Lausanne. His current research activities are in optical metrology, optical fibers and sensors, holography and optical computing, diffractive optical elements, and micro-optics. He was President of the European Optical Society from 1994 to 1996 and is a Vice-President of the International Commission for Optics.

Dr. Dändliker is a Fellow of the Optical Society of America (OSA) and the Swiss Academy of Engineering Sciences, an Honorary Member of the Swiss Society of Optics and Microscopy, and a member of the SPIE, the French Society of Optics, the German Society of Applied Optics, and the European Physical Society.